J. of Electromagn. Waves and Appl., Vol. 25, 2429–2441, 2011

MODELLING EM WAVE INTERACTIONS WITH HUMAN BODY IN FREQUENCY DEPENDENT CRANK NICOLSON METHOD

H. K. Rouf[1,*], F. Costen[2], and M. Fujii[3]

[1]Department of Applied Physics, Electronics and Communication Engineering, University of Chittagong, Chittagong 4331, Bangladesh

[2]School of Electrical and Electronic Engineering, The University of Manchester, Manchester, M60 1QD, UK

[3]Department of Electrical and Electronic Engineering, University of Toyama, Toyama-shi 930-8555, Japan

Abstract—A simulation model of the human body is developed in frequency dependent Crank Nicolson finite difference time domain (FD-CN-FDTD) method. Numerical simulation of electromagnetic wave propagation inside the human head is presented. Advantages of using time discretization beyond the Courant Friedrich-Lewy (CFL) limit in FD-CN-FDTD method are shown. Parallelization using Open Multi-Processing (OpenMP) in a shared memory architecture is performed and the achieved computational efficiencies are shown.

1. INTRODUCTION

With the rapid development of wireless communications technology and the widespread use of mobile phones and other wireless devices there have been increasing public concern about the hazardous effect of electromagnetic radiation on the human body [1]. On the other hand, electromagnetic radiation can be exploited for positive purposes as well. For example, some neurological diseases can be treated using bioelectromagnetic therapy in which certain tissues of the human body are stimulated by electromagnetic fields. Recently researches on the effects of mobile phone radiation on mice suggested that, mobile phones might protect against Alzheimer's diseases [2]. However, there are

* Corresponding author: Hasan Khaled Rouf (hasan_khaled@fuji.waseda.jp).

ethical restrictions on doing experiments on the living human being for studying dosimetry or other bioelectromagnetic aspects. Therefore, numerical simulation is the possible alternative way for this. Out of many numerical methods, the finite difference time domain (FDTD) method is the most suitable technique for this because of its robustness and simplicity.

We have previously proposed frequency dependent Crank Nicolson FDTD (FD-CN-FDTD) method to accommodate frequency dependent materials in unconditionally stable Crank Nicolson FDTD (CN-FDTD) method [12]. The time discretization of CN-FDTD method is not bound by the Courant Friedrich-Lewy (CFL) stability condition of the conventional FDTD method. The FD-CN-FDTD method is based on the original CN-FDTD method which does not make any approximations for computational affordability like the alternating direction implicit (ADI)-FDTD [3] and is, therefore, more accurate.

To model human body references [4, 5] used liquids or gels that simulate the body tissues and fill a container with a regular or an anatomical shape. In such models some researchers used simple single layer structure while others used multilayered structures [6]. However such homogeneous (single layer) and multilayered models cannot represent many of the body regions correctly. Because, for example, the homogeneous model of [7] composed only of the muscle tissues and their multilayered model (three-layer model) consists of skin, fat and muscle tissue layers whereas many inner organs in the human body do not have such symmetric or similar electrical parameters. Several anatomically realistic voxel models of humans have been developed for use in applications of EM dosimetry [8]. With the increase of computing power the resolutions of such models also improved. These models can represent the structural complexities, tissue heterogeneity, and dispersive dielectric properties of human organs quite well. With such voxel models for numerical dosimetry FDTD methods have been used in [9, 10] while parallel FDTD has been used in [11]. Reference [1] attempted to enhance the flexibility of parallel FDTD for bio-electromagnetic problems using an interpolation technique based on domain decomposition parallel FDTD.

However, all these works used conventional or explicit FDTD technique and to our best knowledge no bio-electromagnetic problems have been addressed using implicit FDTD technique. This paper uses implicit FDTD technique, namely CN-FDTD method, for bio-electromagnetic problems. Using the FD-CN-FDTD method a simulation model of the human body is developed. Since electromagnetic properties of the human tissues depend on frequency, accurate numerical studies of EM wave interactions with the human

body requires an FDTD method with the ability of handling frequency dependent media like the FD-CN-FDTD method. The simulation model of the human body uses 2-mm resolution human phantom. Such fine resolution model requires enormously large amount of memory and very long CPU time to do the simulation. One of the ways to overcome these constraints is to parallelise the FD-CN-FDTD code. In this work, parallelization has been done using OpenMP in a shared memory architecture. Computational efficiencies attained through using the time discretization beyond the CFL limit and through using OpenMP are shown. The paper is organized as follows: Section 2 briefly describes the FD-CN-FDTD method. How the human body model is developed in FD-CN-FDTD method is described in Section 3 while numerical simulation of electromagnetic wave propagation inside the human head is shown in Section 4. Computational aspects of these works are presented in Section 5.

2. FREQUENCY DEPENDENT CRANK NICOLSON FDTD METHOD

The FD-CN-FDTD method [12, 13] is briefly described in this section. To implement frequency dependency in the CN-FDTD scheme single-pole Debye media have been used by means of an auxiliary differential formulation [14].

In material independent form, Maxwell's curl equations are

$$\nabla \times \mathbf{E} = -\frac{\partial \mathbf{B}}{\partial t} \tag{1}$$

$$\nabla \times \mathbf{H} = \frac{\partial \mathbf{D}}{\partial t} \tag{2}$$

where $\mathbf{E}$, $\mathbf{H}$, $\mathbf{D}$ and $\mathbf{B}$ are the electric field, magnetic field, electric flux density and magnetic flux density, respectively. In frequency domain, the constitutive relationships for isotropic, linear, non-magnetic, single-pole Debye electrically-dispersive media are

$$\mathbf{B} = \mu_0 \mathbf{H} \tag{3}$$

$$\mathbf{D} = \epsilon_0 + \left(\epsilon_\infty + \frac{\epsilon_S - \epsilon_\infty}{1 + \jmath\omega\tau_D} - \jmath\frac{\sigma}{\omega\epsilon_0} \right) \mathbf{E} \tag{4}$$

where ϵ_0 and μ_0 are the free-space permittivity and permeability, ϵ_S is the static permittivity, ϵ_∞ is the optical permittivity, τ_D is the relaxation time and σ is the static conductivity. Equation Eq. (4) can be re-written as

$$(\jmath\omega)^2 \tau_D \mathbf{D} + \jmath\omega \mathbf{D} = (\jmath\omega)^2 \epsilon_0 \varepsilon_\infty \tau_D \mathbf{E} + \jmath\omega(\epsilon_0 \epsilon_S + \sigma\tau_D)\mathbf{E} + \sigma\mathbf{E} \tag{5}$$

Mapping frequency domain $(jw)^m$ into time domain $\frac{\partial^m}{\partial t^m}$ Eq. (5) can be written as a differential equation in time domain:

$$\tau_D \frac{\partial^2 \mathbf{D}}{\partial t^2} + \frac{\partial \mathbf{D}}{\partial t} = \epsilon_0 \epsilon_\infty \tau_D \frac{\partial^2 \mathbf{E}}{\partial t^2} + (\epsilon_0 \epsilon_S + \sigma \tau_D) \frac{\partial \mathbf{E}}{\partial t} + \sigma \mathbf{E} \tag{6}$$

Application of the Crank-Nicolson method [12] to Eqs. (1)–(3), (6) and algebraic manipulation of the resultant equations yields an equation with only electric field E^{n+1} terms:

$$\begin{aligned} E_x^{n+1} &- \frac{\xi_1}{\xi_4}\left(\frac{\Delta t}{2}\right)^2 \frac{1}{\mu}\frac{\partial^2 E_x^{n+1}}{\partial y^2} + \frac{\xi_1}{\xi_4}\left(\frac{\Delta t}{2}\right)^2 \frac{1}{\mu}\frac{\partial^2 E_y^{n+1}}{\partial x \partial y} + \frac{\xi_1}{\xi_4}\left(\frac{\Delta t}{2}\right)^2 \frac{1}{\mu}\frac{\partial^2 E_z^{n+1}}{\partial z \partial x} \\ &- \frac{\xi_1}{\xi_4}\left(\frac{\Delta t}{2}\right)^2 \frac{1}{\mu}\frac{\partial^2 E_x^{n+1}}{\partial z^2} = \frac{\xi_1}{\xi_4} D_x^n + \frac{\xi_1}{\xi_4}\frac{\Delta t}{2}\frac{\partial H_z^n}{\partial y} + \frac{\xi_1}{\xi_4}\left(\frac{\Delta t}{2}\right)^2 \frac{1}{\mu}\frac{\partial^2 E_x^n}{\partial y^2} \\ &- \frac{\xi_1}{\xi_4}\left(\frac{\Delta t}{2}\right)^2 \frac{1}{\mu}\frac{\partial^2 E_y^n}{\partial x \partial y} - \frac{\xi_1}{\xi_4}\frac{\Delta t}{2}\frac{\partial H_y^n}{\partial z} - \frac{\xi_1}{\xi_4}\left(\frac{\Delta t}{2}\right)^2 \frac{1}{\mu}\frac{\partial^2 E_z^n}{\partial z \partial x} + \frac{\xi_1}{\xi_4}\left(\frac{\Delta t}{2}\right)^2 \frac{1}{\mu}\frac{\partial^2 E_x^n}{\partial z^2} \\ &+ \frac{\xi_1}{\xi_4}\left(\frac{\Delta t}{2}\right)^2 \frac{\partial H_z^n}{\partial y} - \frac{\xi_1}{\xi_4}\left(\frac{\Delta t}{2}\right)^2 \frac{\partial H_y^n}{\partial z} + \frac{\xi_2}{\xi_4} D_x^n + \frac{\xi_3}{\xi_4} D_x^{n-1} - \frac{\xi_5}{\xi_4} E_x^n - \frac{\xi_6}{\xi_4} E_x^{n-1} \end{aligned} \tag{7}$$

Here ξ_1, ξ_2, ξ_3, ξ_4, ξ_5, ξ_6 are space dependent and functions of the Debye parameters and time discretization Δt as defined in [12]. Cyclic permutation of x, y and z in Eq. (7) yields the remaining two E-field equations. By applying them to each grid position in the computational space a system of linear equations of $\mathbf{AN} = \mathbf{C}$ is set up. $\mathbf{A}$ is very large and highly sparse coefficient matrix, $\mathbf{N}$ represents a vector with the electric field components to be solved, and $\mathbf{C}$ is the excitation vector. The system of equations $\mathbf{AN} = \mathbf{C}$ is solved to find the $\mathbf{E}$ field. Then $\mathbf{D}$ and $\mathbf{H}$ fields are calculated in an explicit manner from the $\mathbf{E}$ field. In order to terminate the computational space we employed Mur first order boundary conditions.

3. MODELLING HUMAN BODY IN FD-CN-FDTD

A simulation model of the human body is developed using the FD-CN-FDTD method. In FDTD methods, a numerical model of the human body can be developed by appropriately discretizing the computational space (i.e., human body) and then assigning each discretized space, which represents the tissues and organs, its corresponding dielectric parameters. The dielectric parameters of the human tissues were experimentally measured and compiled by Gabriel et al. in the frequency range of 10 Hz to 20 GHz [15]. Mathematically these parameters, which vary over the frequency, can be modelled by Debye and Cole-Cole models. This work uses the single-pole Debye model

Table 1. Single-pole debye parameters for some human tissues.

Tissue	ϵ_∞	ϵ_S	τ_D (ps)	σ (S/m)
Bladder	9.6746378	19.3315	6.94441	0.30010962
Blood	30.597572	62.9005	7.00378	1.2557440
Bone Cortical	6.6990891	12.9266	10.6297	0.0686324313
Vitreous Humour	4.2372255	69.0152	2.42065	1.5027161

because of its simplicity of implementation in the FDTD method [16]. From Gabriel's data, by using Newton's method and least square fitting technique, the dielectric parameters of the tissues for the Debye model can be obtained [16]. For all the tissues of the human body, the single-pole Debye parameters were obtained and examples of some sample tissue parameters are shown in Table 1.

Advanced medical imaging technology, such as, computed tomography (CT) and magnetic resonance imaging (MRI) can provide high-resolution cross-sectional digital image of the internal anatomy of the human body [17]. When the pixel data obtained from such medical images are extended to three dimensions it gives the cuboidal representation, known as voxels. Voxels can be used to digitally represent the three-dimensional human body. Each voxel contains an uniform volume of the human body such that it can be assigned with an identifying number that corresponds to a particular tissue or organ. Such models are called voxel models or phantoms. In this work the Whole-body Voxel Model of [18] has been used. To model the human body in the FD-CN-FDTD method, the geometrical features of the human body is read from this 2-mm resolution voxel model. The voxel model consists of $320 \times 160 \times 866$ voxels for the male and $320 \times 160 \times 804$ voxels for the female models. However, this work only deals with the male model. For each voxel, that represents a certain tissue, the corresponding single-pole Debye parameters were mapped. In this way, the realistic human body with the frequency dependent dielectric parameters is modelled in FD-CN-FDTD computational space. A cross-section of the human body from this model is shown in Fig. 1. The cross-section is for $z = 57$ plane which lies in the human head (11.4 cm from the top) and has the xy dimensions of 320×160. The area outside the head upto the boundary is free space.

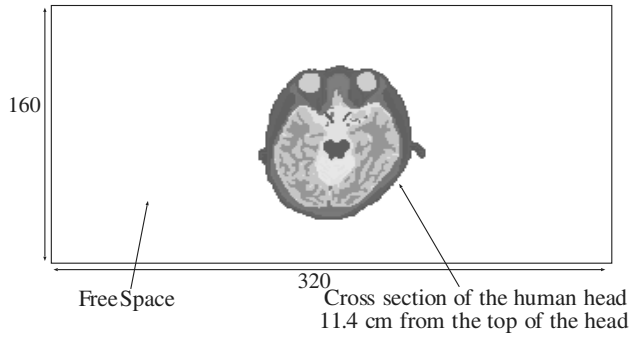

Figure 1. A cross section of the human head at 11.4 cm from the top of the head. The area outside the head upto the boundary is free space.

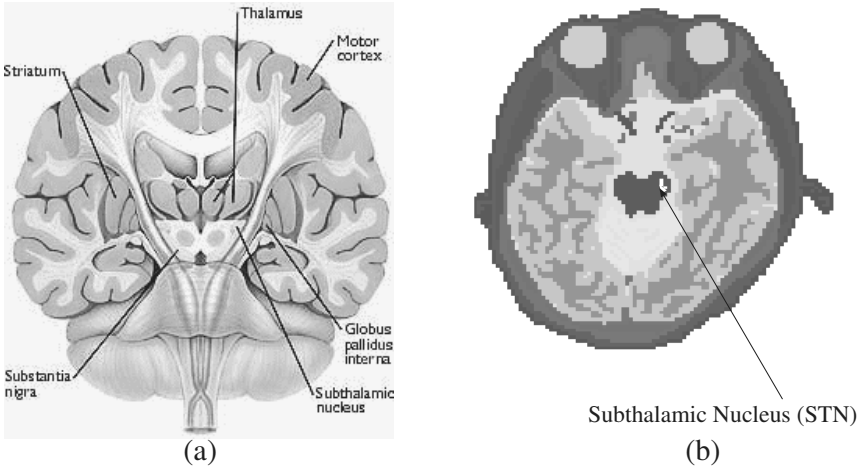

Figure 2. (a) Location of the STN in- side the human head (source: http://www.lloydtan- trust.com/index.php?page=living/sub&type=causation). (b) Location of the STN, inside the human head model, used in the numerical simulation.

4. NUMERICAL TESTS

As a precursor of our future work, here we suggest FD-CN-FDTD's suitability for the research on bioelectromagnetic therapies. We focus on a specific bioelectromagnetic therapy which stimulates subthalamus nucleus (STN) inside the human head to treat Parkinson's disease. STN is a small structure surrounded by several other nuclei and multiple fiber tracts as shown in the left side of Fig. 2. For this work,

it is sufficient to consider the area from the top of the head up to the section above the upper chest in the numerical human body model. Therefore, the size of the FD-CN-FDTD computational space was $320 \times 160 \times 220$ voxels from the top of the head ($220 \times 2\,\text{mm} = 44\,\text{mm}$). By careful calculation, the location of STN was spotted inside the human head model at (169, 86, 57), (169, 87, 57), (170, 88, 57) points as shown in the right side of Fig. 2. In order to resemble the stimulation of STN as in the above bioelectromagnetic therapy, source excitations of z-directed modulated Gaussian pulse centred at 3 GHz were placed at these points. Observations were taken at several points around the head. Based on these observations if source excitations are applied at these points around the head, it would be possible to stimulate the targeted STN by using an appropriate algorithm. Twenty five observation points were chosen around the head with nearly equal distances from one another as shown in Fig. 3. The locations of these twenty five points in the FD-CN-FDTD computational space are given in the table of Fig. 3. It should be pointed out that, the location of the STN is on the $z = 57$ plane and all the twenty five observation points also lie on the $z = 57$ plane. The simulation was run for 1050/CFLN time steps where CFLN $= \Delta t/\Delta t_{\text{CFL}}$; Δt and Δt_{CFL} denotes, respectively, the time discretization in the simulation and the maximum time step size allowed by the CFL stability condition.

Observed signals at the twenty five locations are shown in Fig. 4 for CFLN = 1 and 3. Signals for CFLN = 3 agree well with the corresponding signals for CFLN = 1. Fig. 4 shows that the observed

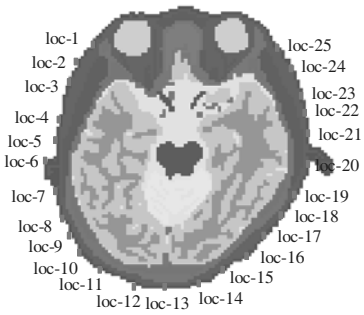

Observation point	*Location in the numerical model*
loc-1	(135, 51, 57)
loc-2	(130, 51, 57)
loc-3	(127, 64, 57)
loc-4	(124, 78, 57)
loc-5	(123, 85, 57)
loc-6	(119, 92, 57)
loc-7	(122, 98, 57)
loc-8	(124, 106, 57)
loc-9	(127, 113, 57)
loc-10	(130, 120, 57)
loc-11	(138, 127, 57)
loc-12	(146, 134, 57)
loc-13	(160, 134, 57)

Observation point	*Location in the numerical model*
loc-14	(175, 134, 57)
loc-15	(180,127, 57)
loc-16	(190, 120, 57)
loc-17	(195, 113, 57)
loc-18	(201, 106, 57)
loc-19	(205, 98, 57)
loc-20	(207, 92, 57)
loc-21	(208, 85, 57)
loc-22	(207, 78, 57)
loc-23	(206, 71, 57)
loc-24	(203, 61, 57)
loc-25	(197, 51, 57)

Figure 3. Locations of the twenty five observation points around the human head model.

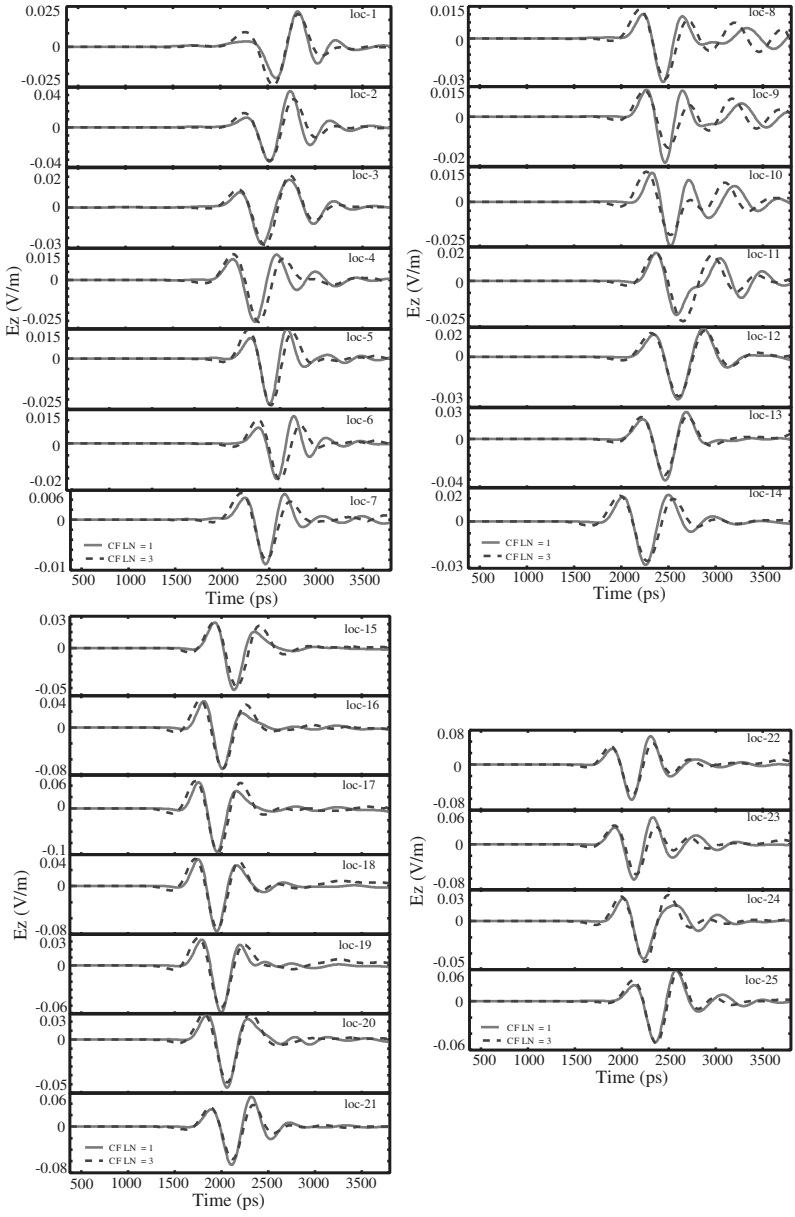

Figure 4. Observed signals at the selected twenty five locations around the human head when CFLN = 1 and 3.

signals are phase shifted from one observation location to the next as expected. Because of the heterogeneities of the tissues of the human head (having different conductivities), the amplitudes of these signals vary a lot from one observation location to the next. The time delays or phase shifts in both cases of CFLN = 1 and CFLN = 3 follow the same pattern. For example, both CFLN = 1 and CFLN = 3 show conspicuous change of phase from loc-12 and loc-18 onward.

Electrical field distributions at different time steps on the $z = 57$ plane in the human head model are shown in Fig. 5 for CFLN = 1 and 3. The electrical field distributions shown in Fig. 5 include the fields in the free space surrounding the head (Fig. 1). To produce Fig. 5, absolute values of the electrical fields were used. Therefore, the minimum values of the electrical field distributions are zero at all the time steps. The changes of electrical field distributions over time inside the human head when CFLN = 1 match quite well with those when CFLN = 3.

5. COMPUTATIONAL EFFICIENCY

The amount of CPU time saved when CFLN = 3 is used instead of CFLN = 1 is shown in Table 2. The efficiency of the simulation of human body model in FD-CN-FDTD method was further improved by parallelization using OpenMP in a shared memory architecture. The OpenMP implementation of FD-CN-FDTD human body model was compiled by Hitachi f90 compiler and run on Hitachi SR16000 Model L2, POWER6 4.7 GHz (dualcore)×16 processors. Table 2 shows the achieved improvement by the OpenMP code over the serial code, in terms of CPU time, when it was run for 1050/CFLN time steps. With the OpenMP code, the CPU time has been greatly reduced when CFLN = 1. We have previously shown in [13] that CPU time is reduced with the increase of CFLN. Obviously, CPU time should be the least when CFLN is the largest (here 3) with OpenMP parallelization. This

Table 2. Speed-up by the OpenMP code on 32 cores at different CFLN.

CFLN=1		
Code type	CPU time	Speed-up
Serial	39 hr 53 min	1
OpenMP	15 hr 11min	2.63

CFLN=3		
Code type	CPU time	Speed-up
Serial	37 hr 38 min	1
Open MP	6 hr 26min	5.85

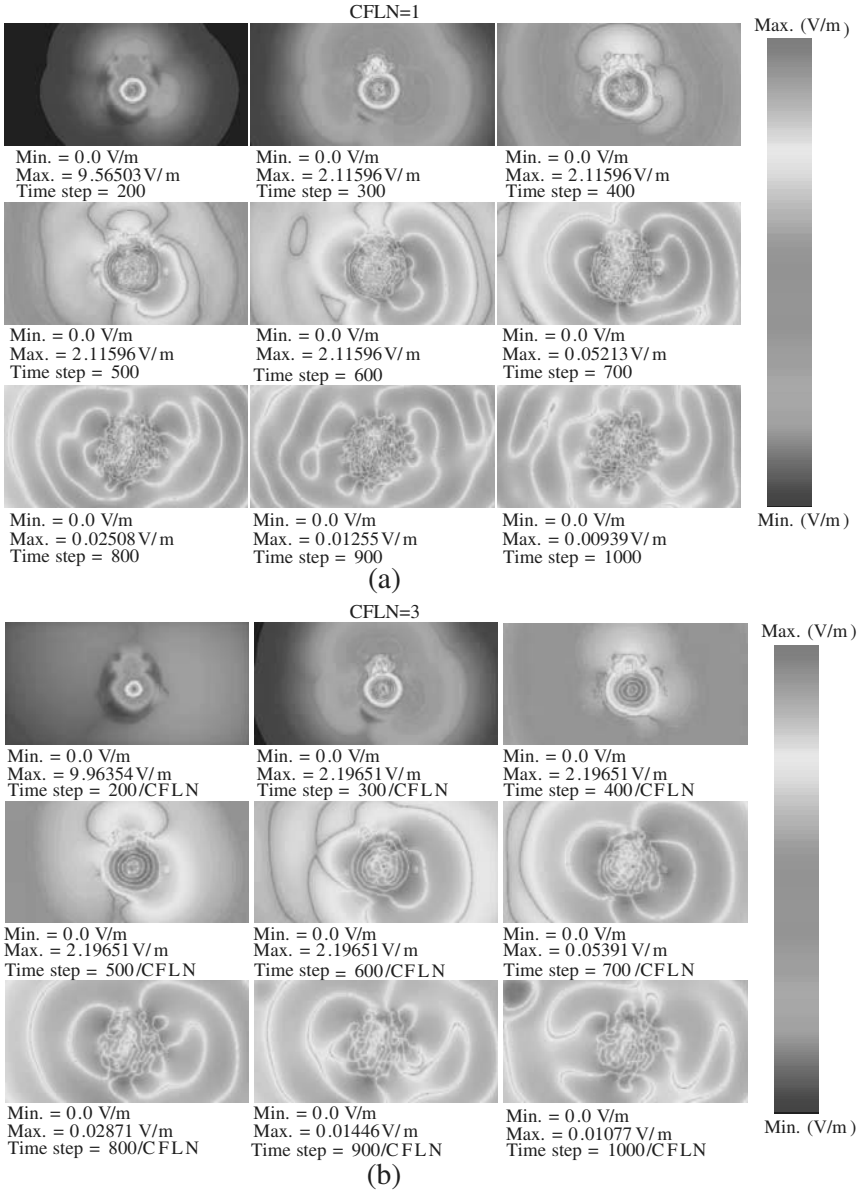

Figure 5. Electrical field distributions at different time steps of the numerical simulation on the $z = 57$ plane within the human head model for CFLN = 1 (a) and CFLN = 3 (b).

is evident in Table 2. However, the scaling is not perfect for the number of threads (32) the code used. In OpenMP, usually, it is hard to obtain perfect speed-ups even when the parallelization is done correctly [19]. Therefore, this performance of the OpenMP code is not very unusual. Understanding the details of underlaying hardware and using vendor-supplied parallel mathematical operation libraries may improve the performance to some extent. But the ultimate benefits of parallelization can be fully achieved by using Message Passing Interface (MPI) in the dynamic memory architecture.

An interesting observation in Table 2 is the increase of speed-up by OpenMP parallelization at higher CFLN. Speed-up by OpenMP for CFLN = 1 and 3 are 2.63 and 5.85, respectively. Further tests with different CFLN need to be performed to check whether the increase of speed-up is always linear with the CFLN. If it is found that better speed-up always comes at higher CFLN, it would indicate that the use of the FD-CN-FDTD method is more appropriate while parallelized (Due to very limited-time access to Hitachi SR16000 Model L2 supercomputer these tests have not yet been performed). At this stage of research it has not yet been confirmed, but this might be resulting from the fact that the operations involved in the increased iteration numbers to converge at higher CFLN (as shown in [13]) are possibly more suitable for parallelization.

6. CONCLUSION

In this paper, we have shown the modelling of human body in FD-CN-FDTD method with all the fine structures and frequency dependent dielectric properties of the human tissues. Numerical simulations of electromagnetic wave propagation inside the human head have been presented. Parallel implementation of the FD-CN-FDTD method in OpenMP has also been presented here. Improvement of CPU time due to higher CFLN and OpenMP has been shown. However, with OpenMP the perfect speed-up was not achieved which is not unusual when parallelisation is done using OpenMP. Future works include the implementation of FD-CN-FDTD method in MPI in the distributed memory architecture to achieve further benefits of parallelization.

ACKNOWLEDGMENT

Thanks to the National Grid Service (NGS), Research Computing Services (RCS) at The University of Manchester, UK and Kyushu University Computing Systems for Research, Japan for their computational resources to run the numerical simulations.

REFERENCES

1. Liu, Y., Z. Liang, and Z. Yang, "Computation of electromagnetic dosimetry for human body using parallel FDTD algorithm combined with interpolation technique," *Progress In Electromagnetics Research*, Vol. 82, 95–107, 2008.
2. Arendash, G., J. Ramos, T. Mori, M. Mamcarz, X. Lin, M. Runfeldt, L. Want, G. Zhang, V. Sava, J. Tan, and C. Cao, "Electromagnetic field treatment protects against and reverses cognitive impairment in alzheimer's disease mice," *Journal of Alzheimer's Disease Propagat.*, Vol. 19, No. 1, January 2010.
3. Garcia, S. G., R. G. Rubio, A. R. Bretones, and R. G. Martin, "On the dispersion relation of ADI-FDTD," *IEEE Microwave and Wireless Components Letters*, Vol. 16, 354–356, June 2006.
4. Chou, H.-H., H.-T. Hsu, H.-T. Chou, K.-H. Liu, and F.-Y. Kuo, "Reduction of peak SAR in human head for handset applications with resistive sheets (R-cards)," *Progress In Electromagnetics Research*, Vol. 94, 281–296, 2009.
5. Karacolak, T., A. Z. Hood, and E. Topsakal, "Design of a dual-band implantable antenna and development of skin mimicking gels for continuous glucose monitoring," *IEEE Transactions on Microwave Theory and Techniques*, Vol. 56, No. 4, 2008.
6. Gemio, J., J. Parron, and J. Soler, "Human body effects on implantable antennas for ISM bands applications: Models comparison and propagation losses study," *Progress In Electromagnetics Research*, Vol. 110, 437–452, 2010.
7. Klemm, M. and G. Troester, "EM energy absorption in the human body tissues due to UWB antennas," *Progress In Electromagnetics Research*, Vol. 62, 261–280, 2006.
8. Hand, J. W., "Modelling the interaction of electromagnetic fields (10 MHz–10 GHz) with the human body: Methods and applications," *Physics in Medicine and Biology*, Vol. 53, 243–286, 2008.
9. Khalatbari, S., D. Sardari, A. A. Mirzaee, and H. A. Sadafi, "Calculating SAR in two models of the human head exposed to mobile phones radiations at 900 and 1800 MHz," *PIERS Online*, Vol. 2, No. 1, 2006.
10. Keshvari, J. and S. Lang, "Comparison of radio frequency energy absorption in ear and eye region of children and adults at 900, 1800 and 2450 MHz," *Physics in Medicine and Biology*, Vol. 50, 4355–4369, 2005.

11. Wang, J. Q., O. Fujiwara, S. Watanabe, and Y. Yamanaka, "Computation with a parallel FDTD system of human-body effect on electromagnetic absorption for portable telephones," *IEEE Transactions on Microwave Theory and Techniques*, Vol. 52, No. 1, 53–58, 2004.
12. Rouf, H. K., F. Costen, and S. G. Garcia, "3-D Crank-Nicolson finite difference time domain method for dispersive media," *Electronics Letters*, Vol. 45, No. 19, 961–962, September 10, 2009.
13. Rouf, H. K., F. Costen, S. G. Garcia, and S. Fujino, "On the solution of 3-D frequency dependent Crank-Nicolson FDTD scheme," *Journal of Electromagnetic Waves and Applications*, Vol. 23, No. 16, 2163–2175, 2009.
14. Joseph, R., S. Hagness, and A. Taflove, "Direct time integration of Maxwell's equations in linear dispersive media with absorption for scattering and propagation of femtosecond electromagnetic pulses," *Optics Lett.*, Vol. 16, No. 18, 1412–1414, 1991.
15. Gabriel, C., "Compilation of the dielectric properties of body tissues at RF and microwave frequencies," *Report N.AL/OE-TR-1996-0037, Occupational and Environmental Health Directorate, Radiofrequency Radiation Division*, Brooks Air Force Base, Texas, USA, June 1996.
16. Wuren, T., T. Takai, M. Fujii, and I. Sakagami, "Effective 2-debye-pole FDTD model of electromagnetic interaction between whole human body and UWB radiation," *IEEE Microwave and Wireless Components Letters*, Vol. 17, No. 7, 2007.
17. Caon, M., "Voxel-based computational models of real human anatomy: A review," *Radiation and Environmental Biophysics*, Vol. 42, No. 4, 2004.
18. Nagaoka, T., S. Watanabe, K. Sakurai, E. Kunieda, S. Watanabe, M. Taki, and Y. Yamanaka, "Development of realistic high-resolution whole-body voxel models of Japanese adult males and females of average height and weight, and application of models to radio-frequency electromagnetic-field dosimetry," *Physics in Medicine and Biology*, Vol. 49, 2004.
19. Chandra, R., R. Menon, L. Dagum, D. Kohr, D. Maydan, and J. McDonald, *Parallel Programming in OpenMP*, Morgan Kaufmann, 2001.